

# Multi-TeV flaring from blazars: Markarian 421 as a case study

Sarira Sahu<sup>1</sup>, Luis Salvador Miranda<sup>1</sup>, Subhash Rajpoot<sup>2</sup>

<sup>1</sup>*Instituto de Ciencias Nucleares, Universidad Nacional Autónoma de México, Circuito Exterior, C.U., A. Postal 70-543, 04510 Mexico DF, Mexico*

<sup>2</sup>*Department of Physics & Astronomy, California State University, 1250 Bellflower Boulevard, Long Beach, CA, 90840, USA*

The TeV blazar Markarian 421 underwent multi-TeV flaring during April 2004 and simultaneously observed in the X-ray and TeV energies. It was observed that the TeV outbursts had no counterparts in the lower energy range, which implies that this might be an orphan flare. We show that Fermi-accelerated protons of energy  $\leq 168$  TeV will interact with the low energy tail of the background synchrotron self-Compton photons in the inner region of the blazar to produce the multi-TeV flare and our results fit very well the observed spectrum. Based on our study, we predict that the blazars with a deep valley in between the end of the synchrotron spectrum and the beginning of the SSC spectrum are possible candidates for orphan flaring. Future possible candidates for this scenario are the HBLs Mrk 501 and PG 1553+113 objects.

## I. INTRODUCTION

Active galactic nuclei (AGN) emit electromagnetic radiation from radio to gamma-rays and exhibit large luminosity variations on time scales ranging from less than an hour up to several years. A super massive black hole is believed to sit at the center of the AGN surrounded by an accretion disk in the inner region and a torus of gas cloud in the outer region. Oppositely directed relativistic jets are ejected from the AGN which are perpendicular to the accretion disk and the torus. In the framework of the unification scheme of AGN, blazars and radio galaxies are intrinsically the same objects, viewed at different angles with respect to the jet axis. When the angle between the jet and the line of sight is small it is called blazar and in contrast, for radio galaxies, the angle between the jet and the light of sight is large. Almost all AGN detected at very high energy (VHE) ( $> 100$  GeV) are blazars with the exception of the three objects, Centaurus A (Cen A)[1, 2], M87 and NGC 1275 which are radio galaxies[3, 4]. The spectral energy distribution (SED) of these AGN have a double peak structure in the  $\nu - \nu F_\nu$  plane. The low energy peak corresponds to the synchrotron radiation from a population of relativistic electrons in the jet. Although the general consensus is that the high energy peak corresponds to the synchrotron self Compton (SSC) scattering of the high energy electrons with their self-produced synchrotron photons, this result remains inconclusive for various reasons. However, the so called leptonic model is very successful in explaining the multi wavelength emission from blazars and FR I galaxies[1–4].

Although the SSC scenario seems to work very well to explain the SED of AGN up to the second peak [5, 6], difficulties arise in explaining the multi-TeV emission detected in Cen A[7], flares from the radio galaxy M87 [8], the flares from blazars 1ES 1959+650[9, 10] and Markarian 421 (Mrk 421)[11]. Also the inevitable outcome of the leptonic scenario is that, emission in multi-TeV energy has to be accompanied by a simultaneously enhanced

emission in the synchrotron peak. Unfortunately the enhanced synchrotron emission was not observed in the flaring of 1ES 1959+650 in June 2002[9] and also probably in the flaring of Mrk 421 in April 2004[11], which implies that the SSC model may not be efficient enough to contribute in the multi-TeV regime.

To explain the orphan flaring of 1ES1959+650 a hadronic synchrotron mirror model was proposed by Böttcher[12]. In this model, the high energy protons from the jet interact with the primary synchrotron photons that have been reflected off clouds located at a few pc above the accretion disk. These photons are blue shifted in the jet frame so that there will be a substantial decrease in the high energy protons to overcome the threshold for  $\Delta$ -resonance. Similarly a structured leptonic jet model is proposed to explain the orphan TeV flare[13].

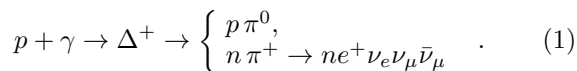
In the hadronic models, the second bump is believed to be formed due to the synchrotron emission from the ultra-high energy protons, or emission from the secondary electron-positron pairs or muons produced from the charged pion decay as a result of the interaction of the high energy protons with the background low energy photons. In this process the decay of neutral pions to  $\gamma$ -ray pairs can explain the high energy peak in the multi-TeV range.

Previously it was shown that the above hadronic processes are inefficient and to explain the high energy peaks efficient acceleration of relativistic protons to ultra-high energies within the inner part of the jet outflow is required. At the same time the jet kinetic power has to exceed the Eddington luminosity by orders of magnitude. The hadronic model is employed by Zdziarski et al.[14] to explain the broad band spectra of radio-loud active galactic nuclei and by Cao et al.[15] to explain the TeV spectrum of the blazar 1ES 1101-232. In both these cases it is shown that super Eddington luminosity in proton is required to explain the high energy peaks. This situation arises because the photon density in the jet is low. However, this problem can be circumvented if one assumes that within the jet there is a dense inner jet region[16]. The multi-TeV peak can also be produced by  $pp$  interac-

tions. It was shown earlier that normally the  $pp$  process is inefficient to produce  $\gamma$ -rays in the blazar environment unless the jet-cloud interaction is taken into account[17–19]. The emission of gamma-rays by the interaction of a population of massive stars surrounding the AGN jets is studied in[20, 21]. Also emission of high energy gamma-rays by the interaction of the AGN jets with the tidally disrupted atmosphere of Red Giant is studied in[22, 23].

## II. PHOTOHADRONIC MODEL

To address the orphan TeV flaring of 1ES 1959+650 and the multi-TeV emission from Cen A and M87, Sahu et al. [16, 24, 25] have used the hadronic model. Recently this model is also used to estimate the neutrinos flux from the TeV-blazars and their spatial correlation with the IceCube events[26]. Here we use the same hadronic model to explain the multi-TeV orphan flaring of Mrk 421. In this model the Fermi-accelerated high energy protons interact with the SSC photons in the core region of the jet (few times the Schwarzschild radius  $R_S$ ) to produce the  $\Delta$ -resonance. Subsequently the  $\Delta$ -resonance decays to charged and neutral pions as follows,



The decay of neutral pions to TeV photons gives the multi-TeV SED. Throughout our work we use natural units  $c = \hbar = 1$ . The relationship between the  $\pi^0$ -decay TeV photon energy  $E_\gamma$  and the target SSC photon energy  $\epsilon_\gamma$  in the observer frame is given by

$$E_\gamma \epsilon_\gamma \simeq 0.032 \frac{\mathcal{D}^2}{(1+z)^2} \text{ GeV}^2, \quad (2)$$

where  $\mathcal{D}$  is the Doppler factor and  $z$  is the redshift. The observed TeV  $\gamma$ -ray energy and the proton energy  $E_p$  are related through

$$E_p = \frac{10\Gamma}{\mathcal{D}} E_\gamma, \quad (3)$$

where  $\Gamma$  is the bulk Lorentz factor of the relativistic jet.

Multi-TeV emission is observed from many blazars and FR I galaxies by Cherenkov telescope arrays. These emission are classified into non-flaring and flaring events. For the non-flaring events (e.g. emission from Cen A[1]), the injected proton spectrum is a power-law given by  $dN_p/dE_p \propto E_p^{-\alpha}$  with  $\alpha \geq 2$ . These protons will interact with the background SSC photons having comoving number density  $n'_\gamma$  (henceforth ' implies the jet comoving frame) and satisfying the kinematical conditions in Eqs.(2) and (3). As discussed in Ref.[16], the flaring occurs within a compact and confined volume of a smaller cone which is enclosed in a bigger cone as shown in Fig. 1. The internal compact jet models are also proposed to explain the fast variability of the blazars Mrk 501 and

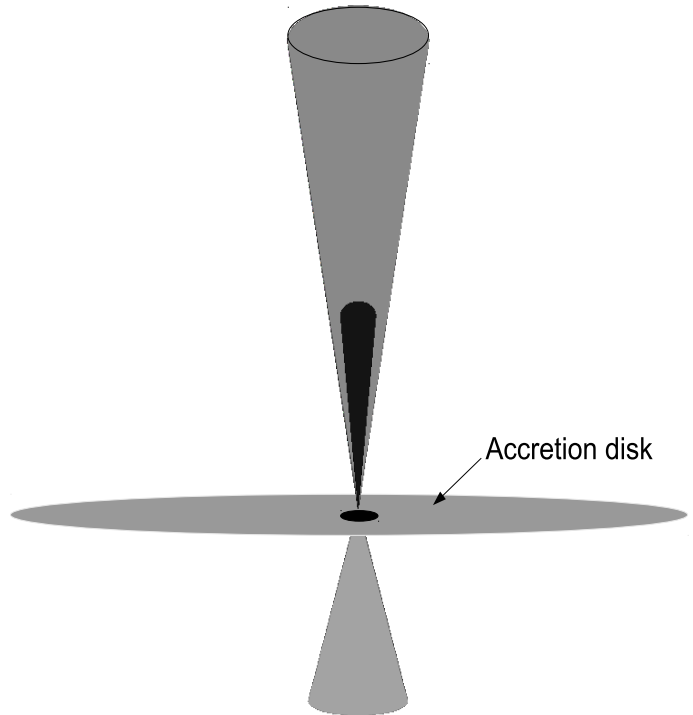


FIG. 1. Geometry of the orphan flaring of blazar Mrk 421: the hidden interior compact cone (jet) is responsible for the multi-TeV orphan flaring and the exterior cone corresponds to the normal jet.

PKS 2155-304[27, 28]. In our case, the injected proton spectrum is a power-law with an exponential decay. In a unified manner we can express the injected proton spectrum for both non-flaring and flaring processes as[16, 29]

$$\frac{dN_p}{dE_p} \propto E_p^{-\alpha} \begin{cases} 1, & \text{non-flaring} \\ e^{-E_p/E_{p,c}}, & \text{flaring} \end{cases}, \quad (4)$$

where  $E_{p,c}$  is the break energy for the high energy protons and above this break energy the proton spectrum falls very fast. The high energy protons will interact in the flaring region having the comoving photon number density  $n'_{\gamma,f}$  to produce the  $\Delta$ -resonance. The photon density in the flaring region is much higher than the rest of the blob (non-flaring region with the photon density  $n'_\gamma$ ) probably due to the copious annihilation of electron positron pairs, splitting of photons in the magnetic field, enhanced IC photons in this region and Poynting flux dominated flow which can form from the magnetic reconnection in the strongly magnetized plasma around the base of the jet[27, 30, 31]. Here we assume that the spectrum has a exponential decay above the  $E_{p,c}$  only for the flaring case. In this model the inner compact region has a size  $R'_f$  smaller than the size of the outer region  $R'_b$  i.e.  $R'_f < R'_b$ . Unfortunately, we do not know exactly the properties of the inner jet except for the number density, the energy density of photons and and the magnetic field are higher than the corresponding values in the outer jet. Due to higher photon density in the inner region, the

multi-TeV  $\gamma$ -rays and neutrinos can be produced through intermediate  $\Delta$ -resonance as shown in Eq. (1). The optical depth of the  $\Delta$ -resonance process in the inner jet region is given by

$$\tau_{p\gamma} = n'_{\gamma,f} \sigma_{\Delta} R'_f. \quad (5)$$

The efficiency of the  $p\gamma$  process depends on the physical conditions of the interaction region, such as the size, distance from the base of the jet, photon density and their distribution in the region.

In the inner region we compare the dynamical time scale  $t'_d = R'_f$  with the  $p\gamma$  interaction time scale  $t'_{p\gamma} = (n'_{\gamma,f} \sigma_{\Delta} K_{p\gamma})^{-1}$  to constraint the seed photon density so that multi-TeV photons can be produced. For a moderate efficiency of this process, we can assume  $t'_{p\gamma} > t'_d$  and this gives  $\tau_{p\gamma} < 2$ , where we take the inelasticity parameter  $K_{p\gamma} = 0.5$ . Also by assuming the Eddington luminosity is equally shared by the jet and the counter jet, the luminosity within the inner region for a seed photon energy  $\epsilon'_\gamma$  will satisfy  $(4\pi n'_{\gamma,f} R'_f \epsilon'_\gamma) \ll L_{Edd}/2$ . This puts an upper limit on the seed photon density as

$$n'_{\gamma,f} \ll \frac{L_{Edd}}{8\pi R'^2_f \epsilon'_\gamma}. \quad (6)$$

From Eq.(6) we can estimate the photon density in this region and this is discussed in Sec. 3. On the other hand, the photon density in the outer region can be calculated from the observed flux. For this we assume a scaling behavior of the photon densities in the flaring and the non-flaring regions which we take to be the following,,

$$\frac{n'_{\gamma,f}(\epsilon'_{\gamma_1})}{n'_{\gamma,f}(\epsilon'_{\gamma_2})} = \frac{n'_\gamma(\epsilon'_{\gamma_1})}{n'_\gamma(\epsilon'_{\gamma_2})}, \quad (7)$$

this implies that, the ratio of photon densities at two different background energies  $\epsilon'_{\gamma_1}$  and  $\epsilon'_{\gamma_2}$  in flaring and non-flaring states remains the same. For a self consistent treatment, in principle we should use the photon density  $n'_{\gamma,f}$  in the hidden internal jet and solve the coupled transport equations for leptons and photons along the jet axis by taking into account their respective cooling mechanisms as well as the injection spectrum of the primary particles[32]. To avoid this complication we assume the scaling behavior of the photon densities in different background energies as shown in Eq. (7). In the photohadronic scenario, the number of  $\pi^0$ -decay photons at a given energy are proportional to both the number of high energy protons and the density of the SSC background photons in the jet, i.e.  $N(E_\gamma) \propto N(E_p)n'_\gamma$ . For the flaring case  $n'_\gamma$  is replaced by the photon density in the flaring region given by  $n'_{\gamma,f}$ . The  $\gamma$ -ray flux from the  $\pi^0$  decay is then given by

$$F_\gamma(E_\gamma) \equiv E_\gamma^2 \frac{dN(E_\gamma)}{dE_\gamma} \propto E_p^2 \frac{dN(E_p)}{dE_p} n'_{\gamma,f}. \quad (8)$$

Using the scaling behavior of Eq.(7), the observed multi-TeV photon flux from  $\pi^0$ -decay at two different observed

photon energies  $E_{\gamma_1}$  and  $E_{\gamma_2}$  can be expressed as

$$\frac{F_\gamma(E_{\gamma_1})}{F_\gamma(E_{\gamma_2})} = \frac{n'_\gamma(\epsilon_{\gamma_1})}{n'_\gamma(\epsilon_{\gamma_2})} \left( \frac{E_{\gamma_1}}{E_{\gamma_2}} \right)^{-\alpha+2} e^{-(E_{\gamma_1}-E_{\gamma_2})/E_c}, \quad (9)$$

where  $E_{\gamma_{1,2}}$  correspond to the proton energy  $E_{p_{1,2}}$ . In this derivation we have used the relations  $E_{p_1}/E_{p_2} = E_{\gamma_1}/E_{\gamma_2}$ , and  $E_{p_{1,2}}/E_{p,c} = E_{\gamma_{1,2}}/E_c$ . By taking the ratio we get rid of the proportionality constant. By using the known flux at a particular energy in the flaring/non-flaring state, we can calculate the flux at other energies using Eq.(9) and also the normalization constant can be calculated.

In terms of SSC photon energy and its luminosity, the photon number density  $n'_\gamma$  is expressed as

$$n'_\gamma(\epsilon_\gamma) = \eta \frac{L_{\gamma,SSC}(1+z)}{\mathcal{D}^{2+\kappa} 4\pi R'^2_b \epsilon_\gamma}, \quad (10)$$

where  $\eta \sim 1$  is the efficiency of SSC process and  $\kappa \sim (0-1)$  depending on whether the jet is continuous or discrete. In this work we consider  $\kappa = 0$ . The SSC photon luminosity is expressed in terms of observed flux ( $\Phi_{SSC}(\epsilon_\gamma) = \epsilon_\gamma^2 dN_\gamma/d\epsilon_\gamma$ ) which is given by

$$L_{\gamma,SSC} = \frac{4\pi d_L^2 \Phi_{SSC}(\epsilon_\gamma)}{(1+z)^2}. \quad (11)$$

Furthermore, by using Eq.(2), we can simplify the ratio of photon densities given in Eq.(7) to

$$\frac{n'_\gamma(\epsilon_{\gamma_1})}{n'_\gamma(\epsilon_{\gamma_2})} = \frac{\Phi_{SSC}(\epsilon_{\gamma_1}) E_{\gamma_1}}{\Phi_{SSC}(\epsilon_{\gamma_2}) E_{\gamma_2}}. \quad (12)$$

Now we can express Eq.(9) in terms of observed SSC flux and  $E_\gamma$  as,

$$\frac{F_\gamma(E_{\gamma_1})}{F_\gamma(E_{\gamma_2})} = \frac{\Phi_{SSC}(\epsilon_{\gamma_1})}{\Phi_{SSC}(\epsilon_{\gamma_2})} \left( \frac{E_{\gamma_1}}{E_{\gamma_2}} \right)^{-\alpha+3} e^{-(E_{\gamma_1}-E_{\gamma_2})/E_c}. \quad (13)$$

Although Eqs.(9) and (13) give the same result, the latter form is much more simpler than the former one. The one in Eq.(13) uses the SED of SSC photon calculated using the leptonic model. Here the multi-TeV flux is proportional to  $E_\gamma^{-\alpha+3}$  and  $\Phi_{SSC}(\epsilon_\gamma)$  while in the former case it is proportional to  $E_\gamma^{-\alpha+2}$  and to the photon number density  $n'_\gamma(\epsilon_\gamma)$ . Finally we would like to point out that in the photohadronic process ( $p\gamma$ ), the multi-TeV photon flux can be expressed as

$$F(E_\gamma) = A_\gamma \Phi_{SSC}(\epsilon_\gamma) \left( \frac{E_\gamma}{TeV} \right)^{-\alpha+3} e^{-E_\gamma/E_c}, \quad (14)$$

where  $A_\gamma$  is a dimensionless constant and both  $\epsilon_\gamma$  and  $E_\gamma$  satisfy the condition given in Eq.(2). This formula will be used to calculate the multi-TeV flux from both non-flaring (without exponential decay term) and flaring events from AGN and their subclass if the emission is

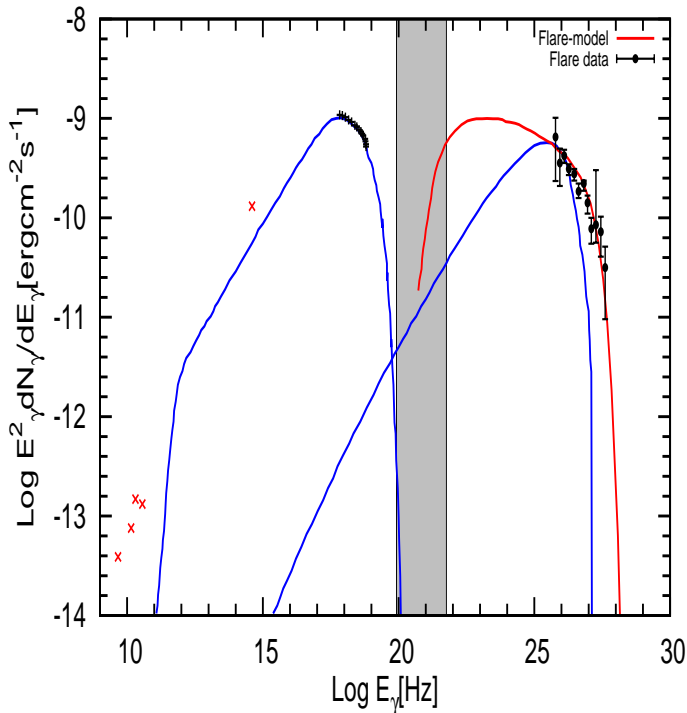


FIG. 2. The SED of Mrk 421 is shown in all the energy bands which are taken from Ref.[11]. The flare of April 2004 in multi-TeV energy is shown here. The hadronic model fit to the April 2004 data is shown as continuous line to the extreme right. The shaded region is the energy range of SSC photons where the Fermi-accelerated protons are collided to produce the  $\Delta$ -resonance.

due to photohadronic process from the core region. For different blazars/AGN, the value of  $A_\gamma$  will be different which we shall discuss in the next section. We can calculate the Fermi accelerated high energy proton flux  $F_p$  from the TeV  $\gamma$ -ray flux through the relation

$$F_p(E_p) = 7.5 \times \frac{F_\gamma(E_\gamma)}{\tau_{p\gamma}(E_p)}. \quad (15)$$

The optical depth  $\tau_{p\gamma}$  is given in Eq.(16). For the observed highest energy proton energy  $E_p$ ,  $F_p(E_p)$  will be smaller than the Eddington flux  $F_{Edd}$ . This condition puts a lower limit on the optical depth of the process and is given by

$$\tau_{p\gamma}(E_p) > 7.5 \times \frac{F_\gamma(E_\gamma)}{F_{Edd}}. \quad (16)$$

From the comparison of different times scales and from Eq.(16) we will be able to constraint the seed photon density in the inner jet region.

### III. MRK 421

Mrk 421 is a high synchrotron peaked BL Lac object (HBL) and is the first extragalactic source with a redshift of  $z=0.031$  to be established as a TeV emitter[33].

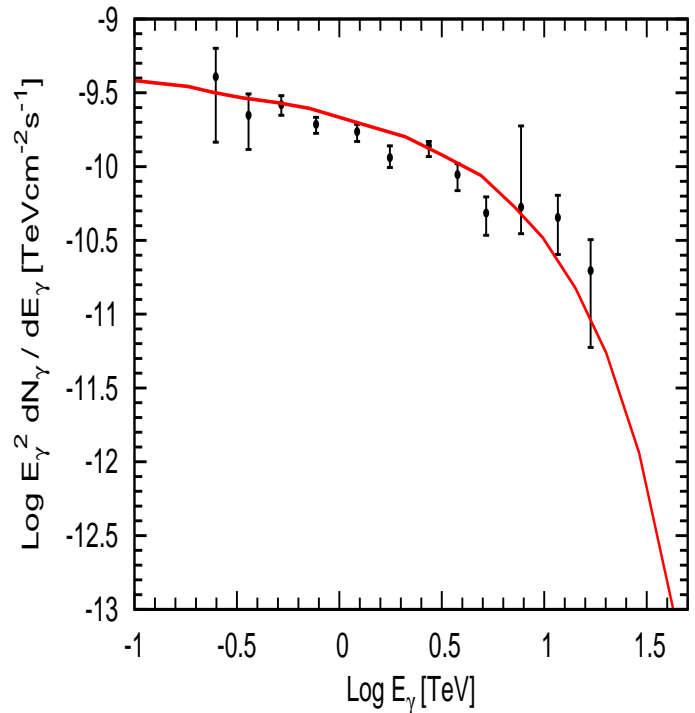


FIG. 3. The continuous curve is the hadronic model fit to the multi-TeV flaring data of Mrk 421.

It has a luminosity distance  $d_L$  of about 129.8 Mpc. Its central supermassive black hole is assumed to have a mass  $M_{BH} \simeq (2 - 9) \times 10^8 M_\odot$  corresponding to a Schwarzschild radius of  $(0.6 - 2.7) \times 10^{14}$  cm and the Eddington luminosity  $L_{Edd} = (2.5 - 11.3) \times 10^{46} \text{ erg s}^{-1}$ . The synchrotron peak of its SED is in the soft to medium X-ray range and the SSC peak is in the GeV range. It is one of the fastest varying  $\gamma$ -ray sources. In the past through dedicated multi wavelength observations, the source has been studied intensively. These studies show a correlation between X-rays and very high energy (VHE)  $\gamma$ -rays. A one-zone SSC model explains the observed SED reasonably well[34]. Several major flares were observed in the 2003/2004 season. During April 2004, a large flare took place both in the X-rays and the TeV energy band. The flare lasted for more than two weeks (from MJD 53,104 to roughly MJD 53,120). But due to a large data gap between MJD 53,093 and 53,104, it is difficult to exactly quantify the duration. The source was observed simultaneously at TeV energies with the Whipple 10 m telescope and at X-ray energies with the Rossi X-ray Timing Explorer (RXTE). It was also observed simultaneously in radio and optical wavelengths. During the flaring it was observed that, the TeV flares had no coincident counterparts at longer wavelengths. Also it was observed that the X-ray flux reached its peak 1.5 days before the TeV flux did during this outburst. So it is believed that, the TeV flare might not be a true orphan flare like the one observed in 1ES 1959+650. On the other hand remarkable similarities between the orphan TeV flare in 1ES 1959+650 and Mrk 421 were observed,

TABLE I. These parameters (up to  $B'$ ) are taken from the one-zone synchrotron model of ref. [11] which are used to fit the SED of Mrk 421. The last three parameters are obtained from the best fit to the observed flare data in our model.

Parameter	Description	Value
$M_{BH}$	Black hole mass	$(2 - 9) \times 10^8 M_\odot$
$z$	Redshift	0.031
$\Gamma$	Bulk Lorentz Factor	14
$\mathcal{D}$	Doppler Factor	14
$R'_b$	Blob Radius	$0.7 \times 10^{16} \text{cm}$
$B'$	Magnetic Field	0.26 G
$R'_f$	Inner blob Radius	$3 \times 10^{15} \text{cm}$
$\alpha$	Spectral index	2.7
$E_c$	$\gamma$ -ray Cut-off Energy	6.2 TeV

including similar variation patterns in X-rays.

By using the one-zone SSC model, the average SED of Mrk 421 is fitted in Fig. 11 of ref. [11]. In Fig. 2 we have shown the SED of Mrk 421. In this figure, the red crosses to the extreme left are the measurements in the radio frequency band measured by 26 m telescope at the University of Michigan Radio Astronomy Observatory (UM-RAO) and by the 13.7 m Metsähovi radio telescope at Helsinki. The single cross (red) in the optical range is measured by Fred Lawrence Observatory (FLWO) 1.2 m telescope. The points of the first peak in the X-ray range are from Rossi X-ray Explorer (RXTE)[11].

In the one-zone leptonic model, the blob of size  $R'_b \sim 0.7 \times 10^{16} \text{cm}$  moves down the conical jet with a Lorentz factor  $\Gamma \simeq 14$  and a Doppler factor of  $\mathcal{D} = 14$ . The emitting region is filled with an isotropic electron population and a randomly oriented magnetic field  $B' = 0.26$  G. In the present work we study the flaring of Mrk 421 during April 2004. We use the parameters of the one-zone leptonic model of ref. [11]. The parameters of the one-zone synchrotron model are summarized in Table I. In principle the Lorentz factor in the inner jet should be larger than the outer jet. But here we assume that  $\Gamma_{out} \simeq \Gamma_{in} \simeq \Gamma$ .

#### IV. RESULTS

The flaring of Mrk 421 in April 2004 was observed in the energy range  $0.25 \text{TeV} (6.0 \times 10^{25} \text{Hz}) \leq E_\gamma \leq 16.85 \text{TeV} (4.1 \times 10^{27} \text{Hz})$  by the Whipple telescope. In the hadronic model discussed above, this corresponds to the Fermi accelerated proton energy in the range  $2.5 \text{TeV} \leq E_p \leq 168 \text{TeV}$  and the corresponding background photon energy will lie in the range  $23.6 \text{MeV} (5.7 \times 10^{21} \text{Hz}) \geq \epsilon_\gamma \geq 0.35 \text{MeV} (8.4 \times 10^{19} \text{Hz})$ . This range of  $\epsilon_\gamma$  is the shaded region shown in Fig. 2 which is in the low energy tail of the SSC photons. For the calculation of normalized multi-TeV flux we take into account one of the observed TeV fluxes from the flare with its corresponding energy and with the use of Eq.(13) calculate other TeV fluxes. In this model the

free parameters are the spectral index  $\alpha$  and the TeV  $\gamma$ -ray cut-off energy  $E_c$  which are adjusted to obtain the best fit and the values are  $\alpha = 2.7$  and  $E_c = 6.2$  TeV. This value of  $E_c$  corresponds to the proton cut-off energy  $E_{p,c} = 62$  TeV and the background SSC photon energy  $\epsilon_{\gamma,SSC} = 0.96 \text{MeV} (2.3 \times 10^{20} \text{Hz})$  which is very close to the beginning of the SSC energy as shown in Fig. 2. This shows that for orphan flaring, the cut-off energy  $E_c$  is due to the change from the synchrotron band to the SSC band and can be calculated from their crossover energy.

In Fig. 3 we show both the observed multi-TeV SED and our model fit to it. In our results, the presence of  $\Phi_{SSC}(\epsilon_\gamma)$  in Eq. (14) modifies the power-law with the exponential fall scenario. From the best fit parameters we obtain the value of the dimensionless constant  $A_\gamma \simeq 20$  in Eq. (14). By using the best fit parameters, we have also calculated the value of  $A_\gamma$  from the multi-TeV flare of 1ES 1959+650 and M87 and the multi-TeV emission from Centaurus A, which are given as 86, 1.86 and  $8.6 \times 10^{-4}$  respectively. We observe that for orphan flaring the condition  $A_\gamma \gg 1$  is satisfied as is seen from 1ES 1959+650 and Mrk421. On the other hand for non-orphan flaring this value is small i.e.  $A_\gamma \leq 1$ .

In the flaring state, the proton luminosity  $L_p$  for the highest observed proton energy  $E_p = 168$  TeV has to be smaller than the  $L_{Edd} \sim 2.5 \times 10^{46} \text{erg s}^{-1}$  and this gives  $\tau_{p\gamma} > 0.02$  in the inner jet region. For our estimates we consider the hidden jet size  $R'_f \simeq 3 \times 10^{15} \text{cm}$  which is between  $R_s$  and the blob radius  $R'_b$ . This value of  $R'_f$  corresponds to a day scale variability. We take day scale variability due to the fact that the flaring lasted for more than two weeks. If we consider small  $R'_f$  then the seed photon density will increase as can be seen from (6). But this increase in density will not affect our results because we are using the scaling behavior of Eq.(7). The constraint on the optical depth gives the lower limit on the seed photon density in the inner region  $n'_{\gamma,f} > 1.3 \times 10^{10} \text{cm}^{-3}$ . Again by assuming  $t'_{p\gamma} < t'_d$  we obtain the upper limit on the optical depth  $\tau_{p\gamma} < 2$  and this corresponds to the photon density  $n'_{\gamma,f} < 1.3 \times 10^{12} \text{cm}^{-3}$ . We have also estimated the seed photon density from Eq.(6), for  $\epsilon_\gamma = 0.35$  MeV, which gives  $n'_{\gamma,f} < 8.9 \times 10^{10} \text{cm}^{-3}$ . The upshot of this analysis is that we get the constraint  $1.3 \times 10^{10} \text{cm}^{-3} < n'_{\gamma,f} < 8.9 \times 10^{10} \text{cm}^{-3}$ , which shows that the photon density in this region is high. This range of photon density corresponds to the optical depth in the range  $0.02 < \tau_{p\gamma} < 0.13$  and the proton flux at  $E_p = 168$  TeV is below the  $F_{Edd} \sim 1.24 \times 10^{-8} \text{erg cm}^{-2} \text{s}^{-1}$ . Due to the adiabatic expansion of the inner blob, the photon density will be reduced to  $n'_\gamma$  and the energy will dissipate once these photons are in the bigger cone. So even if we have two-zones (the inner and the outer), only the outer zone will be responsible for the observed synchrotron and IC peaks. From the leptonic model fit to the SED, the magnetic field in the outer jet region is  $B' = 0.26$  G and

higher magnetic field is expected in the inner jet region. The maximum proton energy in the hidden jet region will be  $E_{p,max} \sim 10^{18}(B'_f/1G)$  eV and for larger magnetic field the  $E_{p,max}$  can even be higher.

In the normal jet scenario we estimate the proton flux needed to explain the observed TeV  $\gamma$ -rays. Corresponding to the background energy  $\epsilon_\gamma = 0.35$  the photon density is  $n'_\gamma \sim 4 \times 10^3 \text{ cm}^{-3}$  and the optical depth is  $\tau_{p\gamma} \sim 1.4 \times 10^{-8}$ . As discussed above, for background SSC photon energy 0.35 MeV, the observed TeV photon has the energy  $E_\gamma = 16.85$  TeV and its flux is  $F_\gamma \sim 3.16 \times 10^{-11} \text{ erg s}^{-1} \text{ cm}^{-2}$ . The high energy proton responsible for the photohadronic process to produce this TeV  $\gamma$ -ray has energy  $E_p = 168$  TeV and we can estimate its flux from Eq.(15) which gives  $F_p \simeq 10^6 \times F_{Edd}$ . This shows that the normal jet model needs super Eddington power in protons to explain the high energy peaks, whereas, the inner jet scenario exterminates this extreme energy requirement.

The high energy protons will be accompanied by high energy electrons in the same energy range. In the magnetic field of the jet, these electrons will emit synchrotron photons in the energy range  $4 \times 10^{19} \text{ Hz}$  to  $2 \times 10^{23} \text{ Hz}$ , which is in the lower part of the SSC spectrum and will not be observable because of the lower flux. Also the SSC emission will take place from these high energy electrons and the energy of these IC photons will be  $E_{IC} \sim \gamma_e^2 \epsilon_{syn}$ . By considering the electron Lorentz factor in the range  $7 \times 10^2 \leq \gamma_e \leq 4 \times 10^4$ [34] and the peak energy of the synchrotron photon  $\epsilon_{syn} \sim 10^{18} \text{ Hz}$ , the SSC process can contribute in the energy range  $2 \text{ GeV} \leq E_{IC} \leq 6.6 \text{ TeV}$ . But the details of the SSC flux depends on the breaks in SSC spectrum and the spectral index. It is observed that during the flaring of Mrk 421, the X-ray emission reached the peak, days after the TeV emission, which poses a serious challenge to the SSC model[11]. The SSC contribution to the multi-TeV band will be very much suppressed. Similarly the multi-TeV photons in the energy range  $0.25 \text{ TeV} \leq E_\gamma \leq 16.85 \text{ TeV}$  can interact with the background photons to produce  $e^+e^-$  pair and these individual electron or positron will have energy  $E_\gamma/2$ . To produce  $e^+e^-$  pair the required threshold seed photon energy  $\epsilon_\gamma \geq 2m_e^2/E_\gamma$  is needed. During the flaring, the multi-TeV  $\gamma$ -rays in the energy range  $0.25 \text{ TeV} \leq E_\gamma \leq 16.85 \text{ TeV}$  will interact with the soft seed photons in the energy range  $0.05 \text{ eV} \leq \epsilon_\gamma \leq 3.5 \text{ eV}$  (in between the infrared and the visible range), where  $\sigma_{\gamma\gamma} \sim 1.7 \times 10^{-25} \text{ cm}^2$  is the maximum cross section and for higher  $\epsilon_\gamma$ , the  $\sigma_{\gamma\gamma}$  will be smaller. The origin of these soft photons are from the synchrotron emission of 1 – 10 GeV electrons in a magnetic field  $\sim 1$  Gauss towards the base of the evolving jet as well as the ambient photons from the disk. On the other hand multi-TeV  $\gamma$ -rays are produced beyond this region where the photons are in the low energy tail (0.35 MeV – 23.5 MeV range) of the IC photons. These two regions are distinct and there will not be enough low energy seed photons (0.05-3.5 eV) in the IC tail region. So, mostly the TeV photons will en-

counter the IC photons and the pair production cross section for  $\epsilon_\gamma \geq 0.35 \text{ MeV}$  is very small  $\sigma_{\gamma\gamma} \leq 10^{-30} \text{ cm}^2$ , which corresponds to a mean free path  $\lambda_{\gamma\gamma} \geq 10^{19} \text{ cm}$ . Hence, TeV photons will not be attenuated much due to  $e^+e^-$  pair production. Also it has been observed that, during the flaring of Mrk 421, the variation in the light curves at optical and radio wavelengths are slight[11], which shows that the low energy photon production was suppressed. The positron produced from the  $\pi^+$  decay will have energy  $E_\gamma/2$  and it will radiate synchrotron photons in the energy range  $2 \times 10^{17} \text{ Hz}$  to  $9 \times 10^{20} \text{ Hz}$ . The photon flux  $F_{e^+,syn}$  from the synchrotron radiation of  $e^+$  will be much smaller than  $F_\gamma(E_\gamma = 0.25 \text{ TeV})/8$ , i.e.,  $F_{e^+,syn} \ll 8 \times 10^{-11} \text{ erg cm}^{-2} \text{ s}^{-1}$ . This flux is well below the observed flux limit in the normal case as can be seen from Fig. 2. From the above analysis our conclusion is that, the photon fluxes from the synchrotron emission of the electrons and positrons are not observable during the flaring event of Mrk 421 in April 2004, which makes this flare orphan, like the one observed in 1ES 1959+650. In principle, the multi-TeV  $\gamma$ -rays from the extragalactic sources can be reduced due to the absorption of TeV photons by the diffuse extragalactic background light (EBL) through the process  $\gamma_{TeV} + \gamma_b \rightarrow e^+e^-$  due to the energy dependent optical depth[35–37]. But for low redshifts and the energy range of our interest, the optical depth does not vary much. Hence we can assume almost a constant optical depth[29] so that the spectral shape remains nearly unchanged.

In conclusion, from the study of the flaring events in blazars, we deduce that the flaring phenomena can be explained through the photohadronic interaction in a compact and confined region within the blazar jet where the photon density is high. From the study of 1ES 1959+650 and Mrk 421, we deduce that orphan flaring can only be possible for those blazars which have a deep valley in between the end of the synchrotron SED and the beginning of the SSC SED as shown in Fig. 2. We note that the HBLs Mrk 501 and PG 1553+113 are possible candidates for orphan flaring in future. For the orphan flaring events we find  $A_\gamma \gg 1$  and for non-orphan flaring  $A_\gamma \leq 1$ .

If Mrk 501 were to produce an orphan flare then the flare energy will lie in the range  $1 \text{ TeV} \leq E_\gamma \leq 8.6 \text{ TeV}$  and this corresponds to the background SSC photon energy in the range  $4.3 \text{ MeV} \geq \epsilon_\gamma \geq 0.5 \text{ MeV}$ . We estimate this by taking the parameters of Mrk 501 as follows:  $\mathcal{D} = 12$ ,  $z = 0.034$  from Ref.[38]. In this case the maximum Fermi-accelerated proton energy will be  $E_p \leq 10E_\gamma \sim 86 \text{ TeV}$ . Also, another condition which must hold for the orphan flaring is

$$A_\gamma = \frac{F(8.6 \text{ TeV})}{\Phi_{SSC}(0.5 \text{ MeV})} \left( \frac{1}{8.6} \right)^{-\alpha+3} e^{8.6/(E_c/\text{TeV})} \gg 1. \quad (17)$$

It has to be noted that, if  $\mathcal{D}$  changes, accordingly the values of  $E_\gamma$ ,  $\epsilon_\gamma$  and the  $E_p$  will also change, but the condition of Eq.(17) is independent of these changes.

## V. CONCLUSIONS

The orphan flaring of Mrk 421 can be explained well by the hadronic model. We observe that, in this model, the multi-TeV photon flux is proportional to  $\Phi_{SSC}(\epsilon_\gamma)$ ,  $E_\gamma^{-\alpha+3}$  and an exponential decay term as shown in Eq. (14). This implies that the Fermi accelerated protons interact with the background photons (in the low energy tail) of the SSC spectrum. During the April 2004 flaring of Mrk 421, we have shown that the flux from the synchrotron emission from the high energy  $e^+$  and  $e^-$  is

suppressed relative to the normal flux implying that the flaring was orphan in nature, like the one observed in 1ES 1959+650. We have also shown what type of blazar spectrum will result in orphan flaring and predict that Mrk 501 and PG 1553+113 are possible candidates for orphan flaring in the future.

Monitoring of these objects by the TeV gamma-ray telescopes will shed more light on the details on the orphan flaring mechanism.

The work of S.S. is partially supported by DGAPA-UNAM (Mexico) Project No. IN110815.

- 
- [1] A. A. Abdo *et al.* [Fermi LAT Collaboration], *Astrophys. J.* **719**, 1433-1444 (2010). [arXiv:1006.5463 [astro-ph.HE]].
- [2] P. Roustazadeh and M. Böttcher, *Astrophys. J.* **728**, 134 (2011).
- [3] G. Fossati, L. Maraschi, A. Celotti, A. Comastri and G. Ghisellini, *Mon. Not. Roy. Astron. Soc.* **299** (1998) 433 [arXiv:astro-ph/9804103].
- [4] G. Ghisellini, A. Celotti, G. Fossati, L. Maraschi and A. Comastri, *Mon. Not. Roy. Astron. Soc.* **301** (1998) 451 [arXiv:astro-ph/9807317].
- [5] C. D. Dermer and R. Schlickeiser, *Astrophys. J.* **416**, 458 (1993).
- [6] M. Sikora, M. C. Begelman and M. J. Rees, *Astrophys. J.* **421**, 153 (1994).
- [7] F. Aharonian *et al.* [HESS Collaboration], *Astrophys. J.* **695**, L40 (2009) [arXiv:0903.1582 [astro-ph.CO]].
- [8] A. Abramowski *et al.* [H.E.S.S. and VERITAS Collaborations], *Astrophys. J.* **746**, 151 (2012) [arXiv:1111.5341 [astro-ph.CO]].
- [9] H. Krawczynski, S. B. Hughes, D. Horan, F. Aharonian, M. F. Aller, H. Aller, P. Boltwood and J. Buckley *et al.*, *Astrophys. J.* **601**, 151 (2004) [astro-ph/0310158].
- [10] W. Cui *et al.* [VERITAS Collaboration], *AIP Conf. Proc.* **745**, 455 (2005) [astro-ph/0410160].
- [11] M. Blazewski, G. Blaylock, I. H. Bond, S. M. Bradbury, J. H. Buckley, D. A. Carter-Lewis, O. Celik and P. Cogan *et al.*, *Astrophys. J.* **630**, 130 (2005) [astro-ph/0505325].
- [12] M. Böttcher, *Astrophys. J.* **621**, 176 (2005) [Erratum-ibid. **641**, 1233 (2006)] [astro-ph/0411248].
- [13] M. Kusunose and F. Takahara, *Astrophys. J.* **651**, 113 (2006) [astro-ph/0607063].
- [14] A. A. Zdziarski and M. Böttcher, *Mon. Not. Roy. Astron. Soc.* **450**, no. 1, L21 (2015) [arXiv:1501.06124 [astro-ph.HE]].
- [15] G. Cao and J. Wang, *Astrophys. J.* **783**, 108 (2014) [arXiv:1401.3970 [astro-ph.HE]].
- [16] S. Sahu, A. F. O. Oliveros and J. C. Sanabria, *Phys. Rev. D* **87**, 103015 (2013) [arXiv:1305.4985 [hep-ph]].
- [17] A. Atoyan and C. D. Dermer, *Phys. Rev. Lett.* **87**, 221102 (2001) [astro-ph/0108053].
- [18] A. M. Atoyan and C. D. Dermer, *Astrophys. J.* **586**, 79 (2003) [astro-ph/0209231].
- [19] C. D. Dermer, K. Murase and H. Takami, *Astrophys. J.* **755**, 147 (2012) [arXiv:1203.6544 [astro-ph.HE]].
- [20] W. Bednarek and R. J. Protheroe, *Mon. Not. Roy. Astron. Soc.* **287**, L9 (1997) [astro-ph/9612073].
- [21] A. Araudo, V. Bosch-Ramon and G. E. Romero, *Mon. Not. Roy. Astron. Soc.* **436**, 3626 (2013) [arXiv:1309.7114 [astro-ph.HE]].
- [22] V. Bosch-Ramon, M. Perucho and M. V. Barkov, *Astron. Astrophys.* **539**, A69 (2012) [arXiv:1201.5279 [astro-ph.HE]].
- [23] M. V. Barkov, F. A. Aharonian, S. V. Bogovalov, S. R. Kelner and D. Khangulyan, *Astrophys. J.* **749** (2012) 119 [arXiv:1012.1787 [astro-ph.HE]].
- [24] S. Sahu, B. Zhang and N. Fraija, *Phys. Rev. D* **85**, 043012 (2012) [arXiv:1201.4191 [astro-ph.HE]].
- [25] S. Sahu and E. Palacios, *Eur. Phys. J. C* **75**, no. 2, 52 (2015) [arXiv:1310.1381 [astro-ph.HE]].
- [26] S. Sahu and L. S. Miranda, *Eur. Phys. J. C* **75**, no. 6, 273 (2015) [arXiv:1408.3664 [astro-ph.HE]].
- [27] D. Giannios, D. A. Uzdensky and M. C. Begelman, *Mon. Not. Roy. Astron. Soc.* **395** (2009) L29 [arXiv:astro-ph/9807317]. arXiv:0901.1877 [astro-ph.HE].
- [28] G. Ghisellini, F. Tavecchio, G. Bodo and A. Celotti, *Mon. Not. Roy. Astron. Soc.* **393**, 16 (2009) [arXiv:0810.5555 [astro-ph]].
- [29] F. Aharonian *et al.* [HEGRA Collaboration], *Astron. Astrophys.* **406**, L9 (2003) [astro-ph/0305275].
- [30] M. Kachelriess, S. Ostapchenko and R. Tomas, *Publ. Astron. Soc. Austral.* **27**, 482 (2010) [arXiv:1002.4874 [astro-ph.HE]].
- [31] D. Giannios, D. A. Uzdensky and M. C. Begelman, *Mon. Not. Roy. Astron. Soc.* **402** (2010) 1649 arXiv:0907.5005 [astro-ph.HE].
- [32] M. M. Reynoso, G. E. Romero and M. C. Medina, *Astron. Astrophys.* **545**, A125 (2012) [arXiv:1208.5284 [astro-ph.HE]].
- [33] M. Punch, C. W. Akerlof, M. F. Cawley, M. Chantell, D. J. Fegan, S. Fennell, J. A. Gaidos and J. Hagan *et al.*, *Nature* **358**, 477 (1992).
- [34] A. A. Abdo *et al.* [MAGIC Collaboration], *Astrophys. J.* **736**, 131 (2011).
- [35] J. D. Finke, S. Razzaque and C. D. Dermer, *Astrophys. J.* **712**, 238 (2010) [arXiv:0905.1115 [astro-ph.HE]].
- [36] A. Dominguez, J. R. Primack, D. J. Rosario, F. Prada, R. C. Gilmore, S. M. Faber, D. C. Koo and R. S. Somerville *et al.*, *Mon. Not. Roy. Astron. Soc.* **410**, 2556 (2011) [arXiv:1007.1459 [astro-ph.CO]].
- [37] Y. Inoue, S. Inoue, M. A. R. Kobayashi, R. Makiya, Y. Niino and T. Totani, *Astrophys. J.* **768**, 197 (2013) [arXiv:1212.1683 [astro-ph.CO]].

- [38] B. Bartoli *et al.* [ARGO-YBJ Collaboration], *Astrophys. J.* **758**, 2 (2012) [arXiv:1209.0534 [astro-ph.HE]].